

Functional Role for the Conformationally Mobile Phenylalanine 223 in the Reaction of Methylenetetrahydrofolate Reductase from *Escherichia coli*^{†,‡}

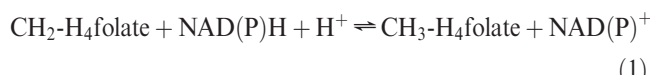
Moon N. Lee,[§] Desire Takawira,[§] Andriana P. Nikolova,[§] David P. Ballou,^{||} Vivek C. Furtado,[⊥] Ngoc L. Phung,[⊥] Brady R. Still,[⊥] Melissa K. Thorstad,[⊥] John J. Tanner,[⊥] and Elizabeth E. Trimmer*,[§]

[§]Department of Chemistry, Grinnell College, Grinnell, Iowa 50112, ^{||}Department of Biological Chemistry, The University of Michigan, Ann Arbor, Michigan 48109, and [⊥]Departments of Chemistry and Biochemistry, University of Missouri—Columbia, Columbia, Missouri 65211

Received April 28, 2009; Revised Manuscript Received July 16, 2009

ABSTRACT: The flavoprotein methylenetetrahydrofolate reductase from *Escherichia coli* catalyzes the reduction of 5,10-methylenetetrahydrofolate ($\text{CH}_2\text{-H}_4\text{folate}$) by NADH via a ping-pong reaction mechanism. Structures of the reduced enzyme in complex with NADH and of the oxidized Glu28Gln enzyme in complex with $\text{CH}_3\text{-H}_4\text{folate}$ [Pejchal, R., Sargeant, R., and Ludwig, M. L. (2005) *Biochemistry* 44, 11447–11457] have revealed Phe223 as a conformationally mobile active site residue. In the NADH complex, the NADH adopts an unusual hairpin conformation and is wedged between the isoalloxazine ring of the FAD and the side chain of Phe223. In the folate complex, Phe223 swings out from its position in the NADH complex to stack against the *p*-aminobenzoate ring of the folate. Although Phe223 contacts each substrate in *E. coli* MTHFR, this residue is not invariant; for example, a leucine occurs at this site in the human enzyme. To examine the role of Phe223 in substrate binding and catalysis, we have constructed mutants Phe223Ala and Phe223Leu. As predicted, our results indicate that Phe223 participates in the binding of both substrates. The Phe223Ala mutation impairs NADH and $\text{CH}_2\text{-H}_4\text{folate}$ binding each 40-fold yet slows catalysis of both half-reactions less than 2-fold. Affinity for $\text{CH}_2\text{-H}_4\text{folate}$ is unaffected by the Phe223Leu mutation, and the variant catalyzes the oxidative half-reaction 3-fold faster than the wild-type enzyme. Structures of ligand-free Phe223Leu and Phe223Leu/Glu28Gln MTHFR in complex with $\text{CH}_3\text{-H}_4\text{folate}$ have been determined at 1.65 and 1.70 Å resolution, respectively. The structures show that the folate is bound in a catalytically competent conformation, and Leu223 undergoes a conformational change similar to that observed for Phe223 in the Glu28Gln– $\text{CH}_3\text{-H}_4\text{folate}$ structure. Taken together, our results suggest that Leu may be a suitable replacement for Phe223 in the oxidative half-reaction of *E. coli* MTHFR.

Methylenetetrahydrofolate reductase (MTHFR)¹ is a flavoprotein that catalyzes the NAD(P)H-dependent reduction of 5,10-methylenetetrahydrofolate ($\text{CH}_2\text{-H}_4\text{folate}$), as shown in eq 1.



The reaction provides $\text{CH}_3\text{-H}_4\text{folate}$, which is the sole methyl donor to homocysteine in the production of methionine by methionine synthase. MTHFR plays a significant role in the homeostasis of homocysteine; mutations in the enzyme lead to

hyperhomocyst(e)inemia (1, 2), which is associated with an increased risk for the development of cardiovascular disease (reviewed in ref 3) and Alzheimer's disease (4–6) in adults and of neural tube defects in the fetus (reviewed in ref 7).

MTHFRs from pig liver, human, *Escherichia coli*, yeast, *Arabidopsis*, and *Leishmania* have been characterized (reviewed in refs 8; (9–12)). Whereas the mammalian and yeast MTHFRs are homodimers in which each subunit contains an N-terminal catalytic domain and a C-terminal regulatory domain to which the allosteric inhibitor adenosylmethionine binds, the *E. coli* enzyme is a homotetramer in which each subunit contains only the catalytic domain. MTHFR enzymes also differ in specificity for NADH or NADPH as the source of reducing equivalents. *E. coli* and plant MTHFRs prefer NADH, whereas the mammalian and yeast enzymes prefer NADPH. Alignment of the *E. coli* sequence with the catalytic region of the human and pig enzymes reveals a 30% level of identity in amino acids, and the accumulated data suggest that the enzymes have a common chemical and kinetic mechanism (13, 14) (K. Yamada, D. P. Ballou, and R. G. Matthews, unpublished results).

MTHFR follows ping-pong bi-bi kinetics (13–15). A flavin adenine dinucleotide (FAD) noncovalently bound to the enzyme serves as an intermediate electron acceptor and donor in the reaction. The FAD accepts reducing equivalents from NAD(P)H in the reductive half-reaction (shown in eq 2). Then in the oxidative half-reaction, the reduced FAD donates its reducing

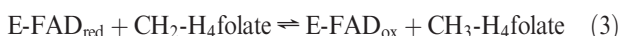
[†]This work was supported in part by American Chemical Society Petroleum Research Fund Grant 39599-GB4 (E.E.T.), by Howard Hughes Medical Institute Undergraduate Biological Sciences Education Grant 71100-503702 (Grinnell College), and by National Institutes of Health Grant GM20877 (D.P.B.). M.K.T. was supported by a Stevens' Summer Undergraduate Research Fellowship from the University of Missouri—Columbia Department of Chemistry.

[‡]Coordinates and structure factors have been deposited in the Protein Data Bank as entries 3FST and 3FSU.

*To whom correspondence should be addressed. E-mail: trimmere@grinnell.edu. Phone: (641) 269-4398. Fax: (641) 269-4285.

¹Abbreviations: $\text{CH}_2\text{-H}_4\text{folate}$, 5,10-methylenetetrahydrofolate; $\text{CH}_3\text{-H}_4\text{folate}$, 5-methyltetrahydrofolate; DHFR, dihydrofolate reductase; EDTA, ethylenediaminetetraacetic acid; E_m , midpoint potential; FAD, flavin adenine dinucleotide; H_2folate , dihydrofolate; H_4folate , tetrahydrofolate; MTHFR, methylenetetrahydrofolate reductase; *p*A_BA, *p*-aminobenzoate; PCA, protocatechuate; PCD, protocatechuate dioxygenase; PDB, Protein Data Bank.

equivalents to the second substrate CH₂-H₄folate, forming the CH₃-H₄folate product and regenerating oxidized FAD (shown in eq 3).



Release of NAD(P)⁺, the product of the first half-reaction, precedes binding of the second substrate, CH₂-H₄folate. Rapid-reaction kinetic studies have demonstrated that MTHFRs from both pig liver and *E. coli* catalyze these individual half-reactions at rates consistent with the observed rates of catalytic turnover (13, 14).

Studies of the porcine enzyme have provided stereochemical and mechanistic details of the MTHFR reaction. Both half-reactions occur as hydride transfers at the *si* face of the FAD (16). In the reductive half-reaction, the *pro*-4S hydrogen of NAD(P)H is removed (17). In the oxidative half-reaction, reduction of the methylene group of CH₂-H₄folate occurs with addition of a hydride to the more sterically accessible face of the pterin (18). However, CH₂-H₄folate, the nitrogen analogue of an acetal, is not well activated for hydride attack. Thus, it has been proposed that, prior to hydride transfer, CH₂-H₄folate is converted to a more reactive 5-iminium cation intermediate by protonation at N10 and concomitant opening of the imidazolidine ring (Scheme 1) (19). Although there is no direct evidence for the existence of a 5-iminium cation in the MTHFR reaction, the intermediate has been postulated to form during the nonenzymatic condensation of formaldehyde and tetrahydrofolate to form CH₂-H₄folate (19). Moreover, a structure of 5-HOCH₂-H₄folate, the product of the reaction of a 5-iminium cation with water, has been obtained in complex with thymidylate synthase, an enzyme that has been proposed to activate CH₂-H₄folate by a mechanism similar to that of MTHFR (20).

Our recent mechanistic studies have focused on MTHFR from *E. coli*. The enzyme modified with a six-histidine tag on the C-terminus has been overexpressed and purified in high yield (14, 21). *E. coli* MTHFR lacks a regulatory domain, so that it is not allosterically regulated by adenosylmethionine, simplifying its kinetic study. Moreover, X-ray structures of bacterial MTHFR, free and ligand-bound, are available (22–24). The enzyme is a tetramer of 33 kDa subunits, each monomer a $\beta_8\alpha_8$ barrel. The FAD cofactor is bound at the C-termini of the β -strands; the isoalloxazine ring lies within the barrel with only its *si* face exposed for reaction (22), in agreement with the known stereochemistry of the reaction (16). Structures of the reduced enzyme in complex with NADH and the oxidized Glu28Gln enzyme in complex with CH₃-H₄folate reveal that the NADH and CH₃-H₄folate ligands occupy partially overlapping sites at the *si* face of the FAD (23). Figure 1 shows a superposition of the NADH (yellow) and folate (white) enzyme complexes. Thus, the binding of one substrate precludes the binding of the other, consistent with the ping-pong bi-bi kinetic mechanism determined

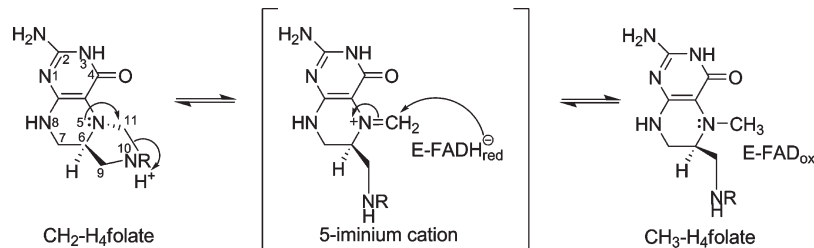
for the enzyme (14). However, within the active site, the conformation of NADH is remarkably different from that of CH₃-H₄folate (Figure 1). The NADH adopts an unusual, highly folded form, stabilized by π - π aromatic stacking interactions. The adenine ring is stacked against Phe223 on one side and against the nicotinamide ring on the other; the nicotinamide is also stacked against the isoalloxazine of the FAD in an orientation that is favorable for hydride transfer. By contrast, CH₃-H₄folate is bound in a more extended conformation: the pterin is stacked against the flavin, the *p*-aminobenzoate (*p*ABA) moiety is perpendicular to the plane of the pterin ring, and the monoglutamate tail extends out from the binding pocket (23).

In this study, we have investigated a possible functional role for amino acid Phe223. The superposition in Figure 1 shows that Phe223 is a conformationally mobile amino acid and assumes distinctly different rotamers in the two complexes (23). In the NADH-bound structure (Figure 1, yellow), the aromatic side chain of Phe223 supports the folded conformation of NADH by stacking against the adenine ring, forming the outer layer of a four-way sandwich. However, in the presence of CH₃-H₄folate (Figure 1, white), the Phe223 side chain has rotated to pack against both the *p*ABA and pterin rings of the folate. Presumably, these interactions are important for maintaining the folate in the catalytically competent conformation in which the pterin ring is parallel to the isoalloxazine. Identification and alignment of MTHFR protein sequences using PsiBlast (25) and Clustal W 2.0 (26, 27), respectively, indicate that Phe223 is not universally conserved despite the key role, inferred from the structures, that this side chain plays in binding both NADH and folate substrates. For example, although Phe occurs at position 223 in most bacterial species, Phe is replaced with a Leu, Met, Ile, or Arg in higher organisms. In fact, the human enzyme contains Leu at the corresponding location.

To test the requirement for an aromatic and/or hydrophobic amino acid at this position, we have constructed the Phe223Leu and Phe223Ala mutants of *E. coli* MTHFR. Harpaz et al. have calculated the mean volumes occupied by residues when buried in the interior of proteins (28). The volume of Leu (164.6 Å³) is comparable to that of Phe (193.5 Å³) (28), suggesting similar hydrophobicity of the residues, yet Leu lacks an aromatic ring and will not be able to participate in π - π interactions with either the NADH or folate substrate. By comparison, Ala has a significantly smaller mean volume (90.1 Å³) (28) than Leu or Phe.

In this paper, we report characterization of the *E. coli* MTHFR mutant enzymes Phe223Leu and Phe223Ala by steady-state and stopped-flow kinetic methods, as well as high-resolution crystal structures of variants Phe223Leu and Phe223Leu/Glu28Gln. Our results support a role for Phe223 in the binding of both the NADH and folate substrates, consistent with our structure-based hypotheses. Moreover, we show that the Phe223Leu mutant is indeed active in folate binding and in catalysis of the oxidative half-reaction.

Scheme 1: Proposed Mechanism for the Oxidative Half-Reaction



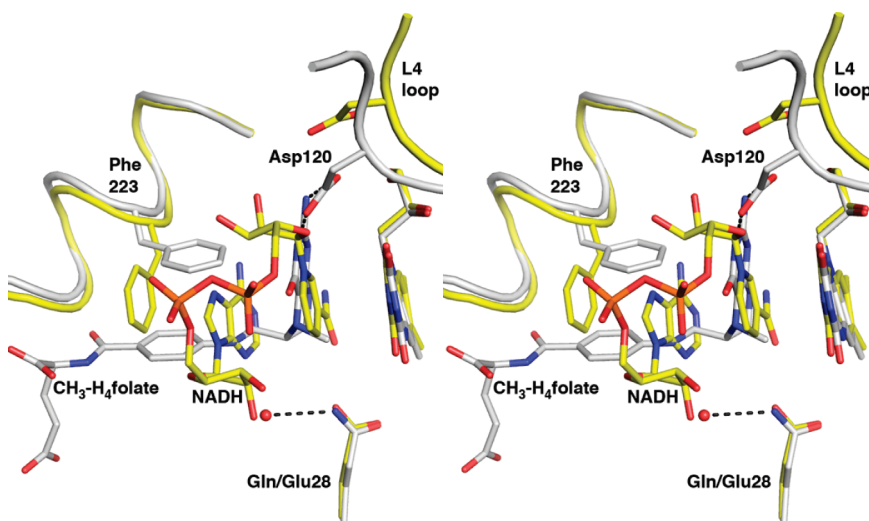


FIGURE 1: Stereographic view of the wild-type MTHFR–NADH complex (yellow, PDB entry 1zpt) and the Glu28Gln MTHFR–CH₃-H₄folate complex (white, PDB entry 1zp4) (23). The ligands occupy partially overlapping sites at the *si* face of the FAD, and residues Asp120, Phe223, and Glu28 (mutated as Glu28) interact with both substrates. The L4 loop moves as a rigid unit to adopt two conformations with different orientations of Asp120. The aromatic side chain of Phe223 adjusts its position to stack either against the adenine ring of the NADH or against the *p*ABA ring of the folate.

EXPERIMENTAL PROCEDURES

Materials. (6*R*)-5,10-CH₂-H₄folate, (6*S*)-H₄folate, and (6*S*)-5-CH₃-H₄folate (sodium salts) were generous gifts from Merck Eprova AG (Schaffhausen, Switzerland). Protocatechuate dioxygenase (PCD) was purified from *Pseudomonas cepacia* DB01 (29) or purchased from Sigma (St. Louis, MO). 3,10-Dimethyl-5-deazaisoalloxazine was a kind gift from V. Massey. The Gene-Tailor Site-Directed Mutagenesis System was purchased from Invitrogen (Carlsbad, CA) and was used with Vent DNA Polymerase from New England BioLabs (Ipswich, MA). Restriction enzymes were obtained from Promega (Madison, WI) or New England BioLabs. T4 DNA ligase and XL1-Blue competent cells were purchased from New England BioLabs and Stratagene, respectively. DNA primers were synthesized by Sigma Genosys (St. Louis, MO). The GENECLEAN kit was obtained from Bio 101 (Vista, CA). Potassium phosphate buffer components and formaldehyde were obtained from Fisher Scientific (Pittsburgh, PA). All other materials were used as purchased from Sigma.

The concentrations of the following solutions were determined spectrophotometrically using an ϵ_{340} of 6220 M⁻¹ cm⁻¹ for NADH (30), an ϵ_{297} of 32000 M⁻¹ cm⁻¹ for CH₂-H₄folate (31), and an ϵ_{340} of 3100 M⁻¹ cm⁻¹ for menadione in methanol (13).

Methods. All experiments were conducted at 25 °C in 50 mM potassium phosphate (pH 7.2) containing 0.3 mM EDTA and 10% glycerol (termed protein buffer). UV-vis measurements were recorded with an Agilent Technologies 8453 diode array spectrophotometer, a Shimadzu UV2401PC double-beam spectrophotometer, or a Cary 50 instrument as indicated below.

Construction of Phe223Leu and Phe223Ala Mutant Plasmids. The Phe223Leu and Phe223Ala mutant plasmids were constructed using the GeneTailor Site-Directed Mutagenesis System (Invitrogen) with minor modifications to the manufacturer's instructions. The pCAS-30 plasmid containing the *E. coli* MTHFR coding sequence juxtaposed with a C-terminal six-histidine tag (21) was methylated with DNA methylase and then used as the template for PCR. Each mutation was introduced using a set of two overlapping, complementary primers, each containing the mutation. The Phe223Leu mutation was created using primers FL2 (5'-CAGGCGAAGAAACTGGCC-

GATATGACC-3') and FL3 (5'-GGTCATATCGGCCAGTT-TCTTCGCCTG-3'), while the Phe223Ala mutation was created using primers FA2 (5'-CAGGCGAAGAAAGCTGCCGA-TATGACC-3') and FA3 (5'-GGTCATATCGGCAGCTTTC-TTCGCCTG-3'). Underlined sequences indicate changes made to introduce the Phe223Leu and Phe223Ala mutations. Vent DNA polymerase (New England BioLabs) was used in the mutagenic PCRs rather than the recommended Platinum High Fidelity Taq Polymerase (Invitrogen). The products of the two PCRs were transformed into *E. coli* host strain DH5α-T1^R (Invitrogen), which circularizes the linear mutated DNA. According to Invitrogen, the success of the procedure relies on the *McrBC* endonuclease within the host cell, which digests the methylated template DNA leaving only the unmethylated, mutated product. The transformants were screened by restriction enzyme digestion. The Phe223Leu mutation created a *Hae*III restriction site, while the Phe223Ala mutation created an *Ahu*I site. DNA sequencing performed by Sequetech (Mountain View, CA) confirmed the sequences of the mutant constructs. The plasmid containing the Phe223Leu mutation was designated pDTL2; the plasmid containing the Phe223Ala mutation was designated pDTA13.

Construction of the Phe223Leu/Glu28Gln MTHFR Plasmid. A mutant plasmid encoding Phe223Leu/Glu28Gln MTHFR was prepared from the two parent plasmids: pDTL2 containing the Phe223Leu mutation and pEET3.10 containing the Glu28Gln mutation (32). Plasmids pDTL2 and pEET3.10 (4470 bp) were digested with restriction enzymes *Xba*I and *Eco*RV to generate 4010 and 460 bp DNA fragments. The pDTL2 4010 bp fragment containing the Phe223Leu mutation and the pEET3.10 460 bp piece containing the Glu28Gln mutation were purified with the GENECLEAN kit and then ligated to generate a 4470 bp expression plasmid, designated pEETQL4. The sequence of the plasmid was verified by restriction enzyme analysis and by DNA sequencing.

Expression and Purification of Mutant Enzymes. Phe223-Leu, Phe223Ala, and Phe223Leu/Glu28Gln histidine-tagged MTHFRs were expressed and purified by the procedures described previously (33). Typically, 12–15 mg of purified

enzyme was obtained from 1 L of bacterial cell culture. The molar extinction coefficients for the mutant enzymes were determined by a method described in a previous paper (33), involving denaturation with guanidine hydrochloride to liberate the bound FAD. Here, the MTHFR enzyme concentration has been expressed as the molarity of enzyme-bound FAD; the enzyme is a tetramer with one molecule of FAD bound per subunit of 34062 Da (21).

Midpoint Potential Determinations. Midpoint potentials of the Phe223Leu and Phe223Ala variants were measured as described for the wild-type enzyme (14), by employing the xanthine/xanthine oxidase reducing system developed by Massey (34) at pH 7.2 and 25 °C in protein buffer. The reference dye was phenosafranine [E_m (pH 7.0) = -252 mV (30), and E_m (pH 7.2) = -258 mV (35)]. UV-vis spectra were recorded on a Shimadzu UV2401PC double-beam spectrophotometer.

Stopped-Flow Kinetic Measurements. All stopped-flow kinetic measurements were taken on a Hi-Tech Scientific model SF-61 stopped-flow spectrophotometer using a tungsten light source for single-wavelength detection (TgK Scientific Ltd., Bradford on Avon, Wiltshire, U.K.). Data acquisition and the instrument were controlled by a computer running Program A (developed in the laboratory of D. P. Ballou). All experiments were performed at 25 °C in protein buffer (pH 7.2) under anaerobic conditions. Prior to use, the instrument was equilibrated overnight in 0.1 M potassium phosphate (pH 7) buffer containing 200 μM protocatechuate (PCA, 3,4-dihydroxybenzoate) and ~0.1 unit/mL protocatechuate dioxygenase (PCD) (36).

Oxidized and reduced enzyme solutions (10 μM, after mixing) were prepared as described in our earlier paper (14) and were maintained at 25 °C during the experiment. Substrate solutions containing various concentrations of NADH or CH₂-H₄folate were made according to the procedures described previously (33). A stock solution of ~20 mM (6R)-5,10-CH₂-H₄folate was prepared anaerobically in protein buffer (pH 8.6) by the addition of a 5-fold molar excess of formaldehyde to (6S)-H₄folate as described previously (33) or by dissolving solid (6R)-5,10-CH₂-H₄folate into protein buffer (pH 8.6) containing a 5-fold molar excess of formaldehyde. PCA (200 μM) and PCD (~0.1 unit/mL) were included in all enzyme and substrate solutions to help maintain anaerobic conditions. Control experiments showed that neither PCA/PCD nor formaldehyde had an effect on the measured rate constants.

Apparent rate constants were calculated from exponential fits of single-wavelength reaction traces in Program A (developed in the laboratory of D. P. Ballou), which uses the Marquardt–Levenberg algorithm (37). Generally, rate constants obtained from three to four shots were averaged, and the error was calculated as the standard deviation from the mean. Often, the values calculated for the observed rate constants were hyperbolically dependent on the substrate concentration. In these cases, the data were fit to eq 4

$$k_{\text{obs}} = \frac{k_{\text{max}}[\text{S}]}{K_d + [\text{S}]} \quad (4)$$

where k_{obs} is the observed rate constant, k_{max} is the maximum rate constant at a saturating substrate concentration, $[\text{S}]$ is the substrate concentration, and K_d is the apparent dissociation constant for the enzyme–substrate complex, using a nonlinear least-squares fitting algorithm in SigmaPlot (SPSS, Inc.). In these

determinations, at concentrations of substrate (15–25 μM) comparable to the enzyme concentration of 10 μM, the reactions are not truly first-order. Thus, simulations were conducted with Global Kinetic Explorer developed by KinTek (Austin, TX), and the observed rate constants were fit to eq 4 to verify apparent K_d values.

Steady-State Kinetic Assays. (i) **NADH–Menadione Oxidoreductase Assay.** MTHFR oxidizes NADH to NAD⁺ in the presence of menadione, and the reaction can be monitored by the decrease in NADH absorbance at 343 nm (38, 39). The assay was performed as described in our earlier paper (14). All reactions were conducted at 25 °C and pH 7.2 in an Agilent Technologies 8453 diode array spectrophotometer using a 0.5 cm path length cuvette. To determine the K_m for NADH, enzyme (final concentration of 0.050 μM) was added to a reaction mixture containing a saturating concentration of menadione (140 μM) and 25–630 μM NADH. Using SigmaPlot, the steady-state kinetic parameters k_{cat} and K_m were determined by fitting the data to the Michaelis–Menten equation (eq 5).

$$\frac{v}{[\text{E}_t]} = \frac{k_{\text{cat}}[\text{S}]}{K_m + [\text{S}]} \quad (5)$$

(ii) **NADH–CH₂-H₄folate Oxidoreductase Assay.** The physiological NADH–CH₂-H₄folate oxidoreductase reaction catalyzed by MTHFR consists of two half-reactions: a reductive half-reaction in which NADH transfers reducing equivalents to the enzyme-bound FAD and an oxidative half-reaction in which the reduced FAD transfers the reducing equivalents to CH₂-H₄folate to generate CH₃-H₄folate. The reaction is observed as a decrease in the NADH absorbance at 340 nm (39, 40). The assay was conducted under anaerobic conditions at 25 °C and pH 7.2, as described previously (14), with the following modification. We employed a Hi-Tech Scientific SFA-20 Rapid Kinetic Accessory (path length of 0.2 cm) attached to a Cary 50 UV-vis spectrophotometer. For use in these experiments, a (6R)-5,10-CH₂-H₄folate stock solution was prepared anaerobically as described above. All solutions contained PCA (100 μM) and PCD (~0.1 unit/mL) to scavenge any remaining oxygen.

To obtain the $K_{m\text{A}}$ for NADH in reactions with the Phe223Leu mutant, the enzyme (0.15 μM after mixing) was mixed with an equal volume of a solution containing 50 μM CH₂-H₄folate and concentrations of NADH varying from 50 to 1500 μM (concentrations after mixing). The $K_{m\text{A}}$ for NADH was calculated by fitting the data to the Michaelis–Menten equation (eq 5). To determine the $K_{m\text{B}}$ for CH₂-H₄folate, the enzyme (0.15 μM) was mixed with an equal volume of a solution containing 1000 μM NADH and concentrations of CH₂-H₄folate varying from 7 to 960 μM (concentrations after mixing). The Phe223Leu variant demonstrated inhibition at concentrations exceeding 100 μM CH₂-H₄folate. To correct the steady-state kinetic constants for this inhibition, the data of varying CH₂-H₄folate concentrations were fit to eq 6 for single-substrate inhibition in a ping-pong bi-bi system (41) using SigmaPlot.

$$\frac{v}{[\text{E}_t]} = \frac{[\text{A}][\text{B}]k_{\text{cat}}}{K_{m\text{A}}[\text{B}](1 + [\text{B}] / K_{i\text{B}}) + K_{m\text{B}}[\text{A}](1 + [\text{A}] / K_{i\text{A}}) + [\text{A}][\text{B}]} \quad (6)$$

NADH–CH₂-H₄folate oxidoreductase reactions with the Phe223Ala mutant were conducted as follows. To determine the $K_{m\text{A}}$ for NADH, the enzyme (0.8 μM) was mixed with an equal volume of a solution containing a saturating concentration of CH₂-H₄folate (400 μM) and concentrations of NADH varying

from 25 to 1000 μM (concentrations after mixing). To determine the K_{mB} for $\text{CH}_2\text{-H}_4\text{folate}$, the enzyme (0.8 μM) was mixed with an equal volume of a solution containing a saturating concentration of NADH (500 μM) and concentrations of $\text{CH}_2\text{-H}_4\text{folate}$ varying from 25 to 800 μM (concentrations after mixing). Both sets of data were fit to the Michaelis–Menten equation (eq 5) to obtain the steady-state kinetic parameters.

Crystallization and Structure Determination. Crystals of Phe223Leu and Phe223Leu/Glu28Gln MTHFR in space group $C2$ were grown using procedures similar to those reported for histidine-tagged wild-type *E. coli* MTHFR and the Glu28Gln mutant (23). Briefly, a 100 μL aliquot of frozen protein (17–20 mg/mL) was thawed and supplemented with 25 μL each of deionized water and 1 mM FAD. Crystals were grown in hanging or sitting drops at room temperature using reservoir solutions of 100 mM sodium cacodylate buffer (pH 5.0–5.5), 225 mM Li_2SO_4 , 5% ethanol, and 10–12% PEG 4000. In preparation for data collection, the pH of the crystals was increased by sequential exchange of the mother liquor with cacodylate-buffered stabilizing solutions at pH 6.0, 7.1, and, finally, 7.4. These stabilizing solutions contained 100 mM sodium cacodylate buffer, 225 mM Li_2SO_4 , 5% ethanol, 15% PEG 4000, and 10% meso-erythritol. The meso-erythritol concentration was then increased to 20% over several minutes. The crystals were then picked up with Hampton mounting loops and plunged into liquid nitrogen.

To form the $\text{CH}_3\text{-H}_4\text{folate}$ complex, a cryoprotected crystal of the Phe223Leu/Glu28Gln enzyme was transferred to a solution of the cryobuffer supplemented with 75 mM (6*S*)-5- $\text{CH}_3\text{-H}_4\text{folate}$ and 20 mM ascorbic acid. After being soaked for 1 h, the crystal was plunged into liquid nitrogen.

Diffraction data were collected at beamline 4.2.2 of the Advanced Light Source and processed with d*TREK (42). The space group is $C2$ with the following unit cell parameters: $a = 103 \text{ \AA}$, $b = 128 \text{ \AA}$, $c = 98 \text{ \AA}$, and $\beta = 122^\circ$. There are three molecules in the asymmetric unit, which corresponds to a solvent content of 57% and a V_m of $2.84 \text{ \AA}^3/\text{Da}$. We note that this crystal form is the same one reported by Guenther et al. (22) and Pejchal et al. (23). Two high-resolution data sets were collected: Phe223Leu– $\text{CH}_3\text{-H}_4\text{folate}$ (1.65 \AA resolution) and Phe223Leu/Glu28Gln– $\text{CH}_3\text{-H}_4\text{folate}$ (1.7 \AA resolution). Data processing statistics are listed in Table 1.

The structures were determined using molecular replacement with the AutoMR utility of PHENIX (45). The search model was derived from chain B of the 1.85 \AA resolution structure of *E. coli* MTHFR Glu28Gln in complex with $\text{CH}_3\text{-H}_4\text{folate}$ (PDB entry 1zp4). Prior to molecular replacement calculations, the side chains of active site residues 219, 223, and 279 were truncated to Ala, all *B*-factors were set to 20 \AA^2 , and the occupancies were set to zero for the $\text{CH}_3\text{-H}_4\text{folate}$ ligand and residues 1–22, 61–69, 120, and 121. Simulated annealing and conjugate gradient refinement were performed with PHENIX (46). COOT was used for model building (47).

Refinement statistics and PDB entries are listed in Table 1. As for other *E. coli* MTHFR structures determined with this $C2$ crystal form, the N-terminal helix (residues 3–21) is disordered in one of the three protein chains of the asymmetric unit. In the structure of the $\text{CH}_3\text{-H}_4\text{folate}$ complex, the folate ligand has been modeled in two of the three chains. In the third chain, a meso-erythritol molecule (used for cryoprotection) occupies the binding site of the folate pterin ring.

Table 1: Data Collection and Refinement Statistics^a

	Phe223Leu	Phe223Leu/Glu28Gln
ligand	none	$\text{CH}_3\text{-H}_4\text{folate}$
space group	$C2$	$C2$
unit cell parameters	$a = 103.1 \text{ \AA}$ $b = 128.2 \text{ \AA}$ $c = 98.3 \text{ \AA}$ $\beta = 122.0^\circ$	$a = 102.9 \text{ \AA}$ $b = 127.9 \text{ \AA}$ $c = 97.6 \text{ \AA}$ $\beta = 121.7^\circ$
wavelength (\AA)	1.000	0.979
diffraction resolution (\AA)	35.0–1.65 (1.71–1.65)	43.7–1.70 (1.76–1.70)
no. of observations	484058	440929
no. of unique reflections	129128	117437
redundancy	3.75 (3.67)	3.75 (3.44)
completeness (%)	99.6 (100.0)	99.8 (99.8)
R_{merge}	0.045 (0.363)	0.033 (0.283)
average I/σ	12.8 (2.4)	18.5 (3.1)
no. of protein chains	3	3
no. of atoms	7104	7097
no. of protein residues	825	829
no. of water molecules	456	400
R_{cryst} ^b	0.210 (0.240)	0.197 (0.238)
R_{free} ^b	0.228 (0.280)	0.220 (0.286)
rmse ^c		
bond lengths (\AA)	0.007	0.006
bond angles (deg)	1.1	1.1
Ramachandran plot ^d		
favored region (%)	99.01	98.77
allowed region (%)	0.62	0.86
outliers (%)	0.37	0.37
average <i>B</i> -factor (\AA^2)		
protein	35	32
FAD	27	27
ligand	not available	38
water	35	31
PDB entry	3FST	3FSU

^a Values for the outer resolution shell of data are given in parentheses.

^b A 5% test set. A common set of test reflections was used for refinement of all structures. ^c Root-mean-square deviation, compared to the parameters of Engh and Huber (43). ^d The Ramachandran plot was generated with RAMPAGE (44).

RESULTS

Spectral and Redox Properties of the Phe223Leu and Phe223Ala Mutants Are Similar to Those of Wild-Type MTHFR. The Phe223Leu and Phe223Ala mutant enzymes were purified with FAD bound, using the same procedures used for wild-type MTHFR (14, 33). The visible absorbance spectrum of the Phe223Leu enzyme (Figure 2) is essentially identical to that of the wild-type enzyme. By contrast, a small shoulder near 345 nm is present in the spectrum of the Phe223Ala variant (Figure 2). The wavelength of maximal absorbance (447 nm) and the molar extinction coefficient ($14300 \text{ M}^{-1} \text{ cm}^{-1}$) of the mutants are unchanged from those determined for the wild-type enzyme (14). Like wild-type MTHFR (14), the mutants are nonfluorescent.

Changes in the amino acids near a flavin often cause alterations in the midpoint potential of the bound flavin. The two-electron midpoint potentials of the Phe223Leu and Phe223Ala enzymes were measured at pH 7.2 and 25 °C using a method described by Massey (34). Phenosafranine with a midpoint potential of -258 mV at pH 7.2 was employed as the reference dye. Consistent with the rather long distance from Phe223 to the FAD in MTHFR [$\sim 13 \text{ \AA}$ between the α -carbon of position 223 and N5 of FAD (23)], the midpoint potentials of the mutants were not significantly altered compared to that of the wild-type enzyme (Table 2).

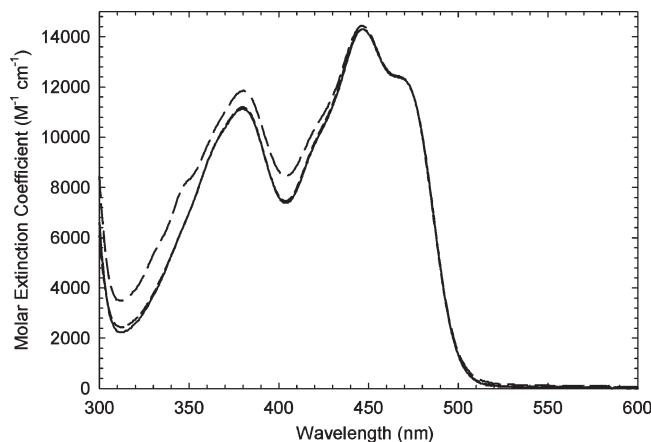


FIGURE 2: Spectra of purified Phe223 mutant and wild-type MTHFR enzymes: Phe223Leu (—), Phe223Ala (---), and wild-type (---) enzymes ($30 \mu\text{M}$) in 50 mM potassium phosphate (pH 7.2) buffer containing 0.3 mM EDTA and 10% glycerol. For all enzymes, the wavelength of maximal absorbance is 447 nm and the molar extinction coefficient is $14300 \text{ M}^{-1} \text{ cm}^{-1}$.

The Structure of Phe223Leu MTHFR Resembles That of the Wild-Type Enzyme. The crystal structure of Phe223Leu MTHFR was determined to assess the impact of the mutation on the structure of the active site (Table 1). The structure of the ligand-free Phe223Leu variant was determined at 1.65 \AA resolution. As expected, the mutant displays the $(\beta\alpha)_8$ fold and the FAD cofactor is bound at the C-terminal ends of the barrel strands (Figure 3A), as described previously for MTHFR (23). The overall structures of Phe223Leu and wild-type MTHFR are quite similar. The pairwise root-mean-square deviations (rmsds) between the three chains of the Phe223Leu asymmetric unit and those of the wild-type enzyme (PDB entry 1zp3) (23) are $0.15\text{--}0.51 \text{ \AA}$ (for C_α atoms). For reference, the rmsds between chains of the asymmetric unit of the wild-type structure span the range of $0.44\text{--}0.54 \text{ \AA}$. Thus, within experimental error, Phe223Leu is identical to the wild-type enzyme at the fold level.

The active sites of Phe223Leu and wild-type MTHFR are also quite similar. As shown in Figure 3B, several side chains in the active sites of the two enzymes superimpose nearly perfectly, including Asp120 of the flexible L4 loop, the catalytic residue Glu28, the folate-binding residue Gln183, and several nonpolar residues. Mutation of Phe223 to Leu causes minimal disruption. Leu223 and Phe223 have nearly identical χ_1 values (ca. -70°); thus, their C_γ atoms overlap (Figure 3B).

The Affinity for NADH Is Decreased Significantly by the Phe223Leu and Phe223Ala Mutations. We have hypothesized that Phe223 would participate in NADH binding and possibly catalysis, based on the significant π -stacking interactions between the Phe side chain and NADH. To investigate the reductive half-reaction, the oxidized mutant forms were mixed with NADH under anaerobic conditions in a stopped-flow spectrophotometer at 25°C . The Phe223Leu and Phe223Ala enzymes behaved qualitatively in a similar manner. At 450 nm, the traces showed a decrease in absorbance in a single phase. At wavelengths between 550 and 750 nm, no transient absorbance typical of flavin-NAD(H) charge-transfer complexes was detected during reduction. These results stand in contrast to a clear E_{ox} -NADH charge-transfer complex observed at 550–650 nm during the reduction reaction of wild-type MTHFR (14). Scheme 2 diagrams a minimal kinetic scheme for the reductive half-reaction.

The 450 nm reaction traces for the Phe223Leu mutant were fit to one exponential phase (Figure 4). The observed rate constants for flavin reduction were hyperbolically dependent on the concentration of NADH (inset of Figure 4). A fit of the data to eq 4 yielded a maximal observed rate constant for reduction of $35 \pm 1 \text{ s}^{-1}$, a decrease of less than 2-fold compared to the analogous value for wild-type MTHFR, and an apparent K_d for NADH of $440 \pm 20 \mu\text{M}$, a significant (14-fold) increase over that for the wild-type enzyme (Table 2). The reductive half-reaction of the Phe223Ala mutant was also examined in the stopped-flow spectrophotometer. The reaction traces were monophasic. The observed rate constants exhibited a hyperbolic dependence on NADH concentration with a maximal observed rate constant for reduction of $40 \pm 2 \text{ s}^{-1}$ and an apparent K_d for NADH of $1340 \pm 100 \mu\text{M}$ (Table 2), a 40-fold increase over the K_d for the wild-type enzyme. Thus, mutation of Phe223 to either Leu or Ala significantly lowers the apparent affinity for NADH. However, the rate of reduction of FAD by NADH has been only minimally affected by these mutations.

In the Steady-State NADH–Menadione Oxidoreductase Assay, the Phe223Leu and Phe223Ala Variants Have Larger K_m Values for NADH than Wild-Type MTHFR. Under aerobic conditions, *E. coli* MTHFR catalyzes the NADH–menadione oxidoreductase reaction shown in eq 7.



This reaction consists of two half-reactions: a reductive half-reaction in which the FAD is reduced by NADH and an oxidative half-reaction in which the reduced FAD is reoxidized by menadione, an artificial electron acceptor. The assay was performed with the Phe223Leu and Phe223Ala mutant enzymes in the presence of a saturating level of menadione ($140 \mu\text{M}$). In the stopped-flow spectrophotometer, the reaction of reduced Phe223Leu and Phe223Ala enzymes with $140 \mu\text{M}$ menadione is very fast, occurring within the 3 ms dead time of the instrument (data not shown). Thus, in the NADH–menadione oxidoreductase assay, the rate is limited fully by the reductive half-reaction with NADH.

The assay was conducted with the Phe223Leu enzyme at $140 \mu\text{M}$ menadione and varying NADH concentrations at 25°C and pH 7.2. A fit of the data to the Michaelis–Menten equation (eq 5) gave a maximum turnover number (k_{cat}) of $31 \pm 4 \text{ s}^{-1}$ and a K_m for NADH of $470 \pm 115 \mu\text{M}$ (Table 3), the latter an increase of 7-fold compared to that of the wild-type enzyme (14). The NADH–menadione oxidoreductase assay was also performed with the Phe223Ala mutant enzyme. From our data, we determined k_{cat} and K_m for NADH to be $22 \pm 4 \text{ s}^{-1}$ and $585 \pm 200 \mu\text{M}$, respectively (Table 3). Thus, K_m for NADH has been increased 7–9-fold in the Phe223Leu and Phe223Ala variants.

Taken together, the stopped-flow and steady-state data suggest that the Phe223Leu and Phe223Ala variants are only slightly hindered in their reduction by NADH. By contrast, the K_d results indicate that the mutations have significantly weakened the ability of MTHFR to bind the NADH substrate. Consistent with the lower affinity of the Phe223Leu variant for NADH, attempts to capture a Phe223Leu–NADH complex have been unsuccessful using the crystal soaking procedure described for the wild-type enzyme (23). Although weak electron density suggestive of a folded NADH molecule bound to the Phe223Leu enzyme was obtained, refinement of the model was unsatisfactory, indicating low occupancy and possibly multiple conformations of the ligand.

Table 2: Midpoint Potential and Rapid-Reaction Kinetic Constants ^a			
	Phe223Leu	Phe223Ala	wild type ^b
midpoint potential (mV)	-240 ± 3	-236 ± 3	-237 ± 4
reductive half-reaction			
with NADH ^c			
k_2' (s ⁻¹)	35 ± 1	40 ± 2	55 ± 6
K_d for NADH (μM)	440 ± 20	1340 ± 100	32 ± 5
oxidative half-reaction with			
CH ₂ -H ₄ folate ^d			
k_5' (s ⁻¹)	34 ± 1	4.5 ± 1.1 ^e	10.3 ± 1.0 ^e
K_d for CH ₂ -H ₄ folate (μM)	9 ± 2	500 ± 230	11 ± 1

^aAll measurements were taken at 25 °C in 50 mM potassium phosphate buffer (pH 7.2) containing 0.3 mM EDTA and 10% glycerol. ^bFrom ref 14. ^cDefinition of rate constants given in Scheme 2. The net rate constant for reduction, k_2' , is defined as $k_2' = (k_2 k_3)/(k_{-2} + k_3)$ (48). ^dDefinition of

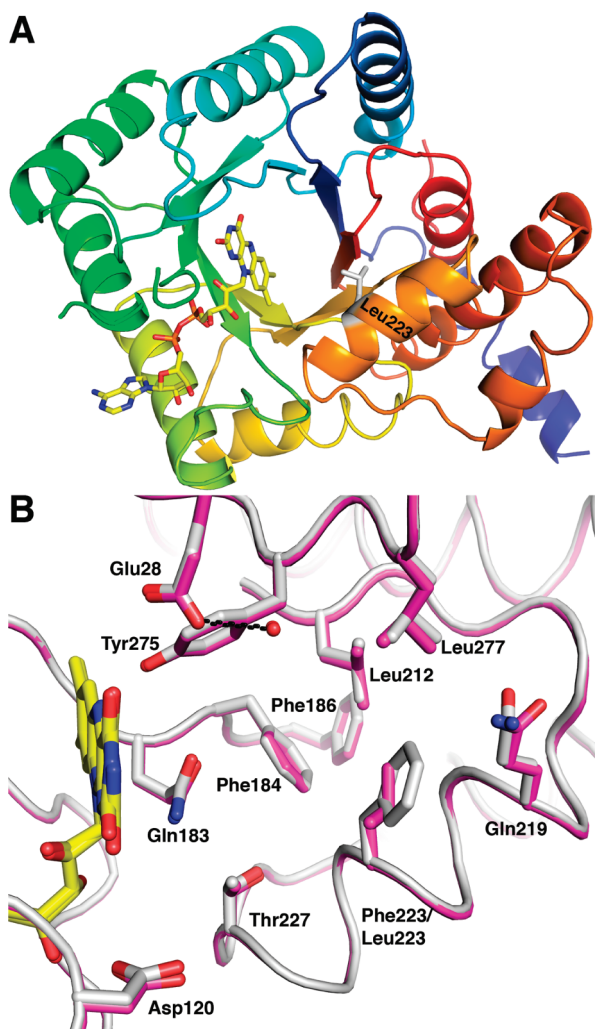


FIGURE 3: Structures of Phe223Leu MTHFR. (A) Ribbon drawing of Phe223Leu MTHFR. The protein is colored in a rainbow scheme, with blue at the N-terminus and red at the C-terminus. The FAD is drawn as yellow sticks. The side chain of Leu223 is colored white. (B) Comparison of the active sites of Phe223Leu (magenta) and wild-type MTHFR (white, PDB entry 1zp3). The FAD cofactors of both enzymes are colored yellow.

Compared to That of Wild-Type MTHFR, the Rate of Reaction with CH₂-H₄folate Is Increased by the Phe223-Leu Mutation but Decreased by the Phe223Ala Mutation.

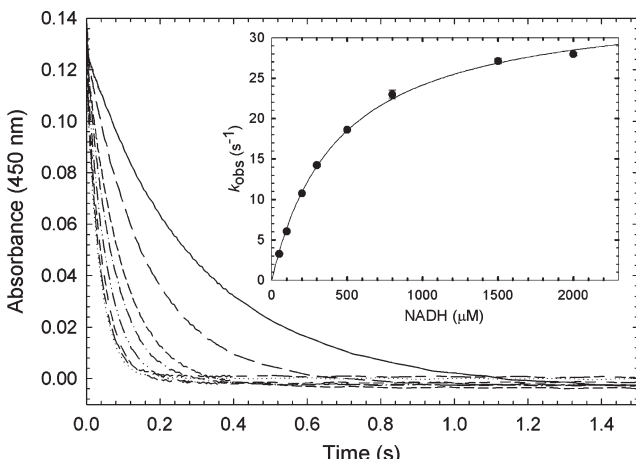
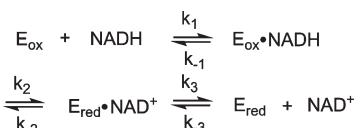


FIGURE 4: Reduction of the Phe223Leu enzyme by NADH. The oxidized enzyme, 10 μM, was mixed with solutions of 50 (—), 100 (---), 200 (---), 300 (---), 500 (---), 800 (---), 1500 (---), and 2000 μM (···) NADH (concentrations after mixing). Stopped-flow reaction traces were monitored at 450 nm. The reaction was monophasic. The inset shows the dependence of the observed rate constant for reduction on NADH concentration. The data were fit to a hyperbolic equation (eq 4), which yielded an apparent K_d of 440 ± 20 μM for NADH and a maximum rate constant for reduction (k_2' , according to Scheme 2) of 35 ± 1 s⁻¹. Reaction conditions were 50 mM potassium phosphate (pH 7.2) buffer containing 0.3 mM EDTA and 10% glycerol at 25 °C.

Scheme 2: Kinetic Mechanism for the Reductive Half-Reaction



Stacking between the aromatic rings of Phe223 and the pABA moiety of CH₂-H₄folate (Figure 1) suggests a role for this amino acid in folate binding and catalysis. The oxidative half-reactions of the Phe223Leu and Phe223Ala mutant forms were examined in a stopped-flow apparatus at 25 °C and pH 7.2. When the photoreduced Phe223Leu enzyme was reacted with CH₂-H₄folate under anaerobic conditions, an increase in flavin absorbance at 450 nm was observed (Figure 5). The reaction traces appeared monophasic and were fit to one exponential phase. This is in contrast to the biphasic kinetics observed for wild-type MTHFR at 25 °C (14). The data for the variant depended on the concentration of CH₂-H₄folate in a hyperbolic manner (inset of Figure 5). A fit of the data to eq 4 yielded an apparent K_d for CH₂-H₄folate of 9 ± 2 μM, which is similar to the value of 11 ± 1 μM obtained for wild-type MTHFR (14), and a maximal rate constant of 34 ± 1 s⁻¹ (Table 2), a 3-fold increase compared to that reported for the slow phase of the wild-type enzyme (14). Because in the experiment, first-order conditions were not achieved at substrate concentrations of 17 and 25 μM (the enzyme concentration was 10 μM), simulations were performed with the KinTek Global Kinetic Explorer program (available as Supporting Information). The oxidative half-reaction of the Phe223Leu variant was modeled with the mechanism shown as Scheme 3 for CH₂-H₄folate concentrations of 17–300 μM. The following rate constants reasonably modeled our experimental data: $k_4 = 7 \mu\text{M}^{-1} \text{s}^{-1}$, $k_{-4} = 56 \text{s}^{-1}$, $k_5 = 29 \text{s}^{-1}$, $k_{-5} = 14 \text{s}^{-1}$, $k_6 = 1018 \text{s}^{-1}$, and $k_{-6} = 9 \mu\text{M}^{-1} \text{s}^{-1}$. The simulated traces (see the Supporting Information) were fit to one exponential phase,

Table 3: Steady-State Kinetic Constants^a

	Phe223Leu	Phe223Ala	wild type ^b
NADH–menadione			
oxidoreductase assay			
k_{cat} (s ⁻¹)	31 ± 4	22 ± 4	55 ± 8.3
K _m for NADH (μM)	470 ± 115	585 ± 200	66 ± 16
NADH–CH₂-H₄folate			
oxidoreductase assay			
k_{cat} (s ⁻¹)	14 ± 2	2.9 ± 0.5	10.4 ± 1.0
K _m for NADH (μM)	236 ± 36	140 ± 7	20 ± 4
K _m for CH ₂ -H ₄ folate (μM)	8 ± 2	93 ± 16	0.5 ± 0.1
K _i for CH ₂ -H ₄ folate (μM)	160 ± 27	nd ^c	320 ± 25

^aKinetic constants were determined at 25 °C in 50 mM potassium phosphate buffer (pH 7.2) containing 0.3 mM EDTA and 10% glycerol.

^b From ref 14. ^c Not able to be determined.

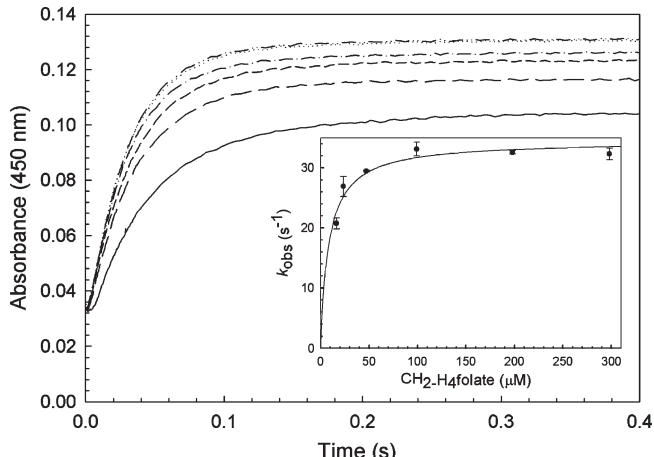
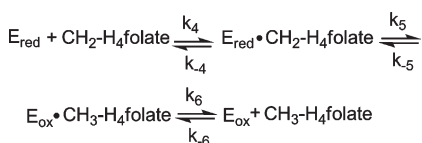


FIGURE 5: Reoxidation of the reduced Phe223Leu enzyme by CH₂-H₄folate. Photoreduced enzyme (10 μM) was mixed with solutions of 17 (—), 25 (---), 50 (--) 100 (-·-), 200 (-··-), and 300 μM (····) CH₂-H₄folate (concentrations after mixing). Stopped-flow reaction traces, monitored at 450 nm, were monophasic. The inset shows the dependence of the observed rate constant on CH₂-H₄folate concentration. A fit of the data to eq 4 yielded an apparent K_d for CH₂-H₄folate of $9 \pm 2 \mu\text{M}$ and a maximal rate constant for oxidation ($k_{5'}$, according to Scheme 3) of $34 \pm 1 \text{ s}^{-1}$. Reaction conditions were 50 mM potassium phosphate (pH 7.2) buffer containing 0.3 mM EDTA and 10% glycerol at 25 °C.

Scheme 3: Kinetic Mechanism for the Oxidative Half-Reaction



and the observed rate constants showed a hyperbolic dependence on the concentration of CH₂-H₄folate, giving an apparent K_d for CH₂-H₄folate of $13 \pm 1 \mu\text{M}$ and a maximal observed rate constant for oxidation of $36 \pm 1 \text{ s}^{-1}$, values similar to those obtained experimentally.

Figure 6 shows the reaction traces at 450 nm associated with the reoxidation of the reduced Phe223Ala enzyme by CH₂-H₄folate at 25 °C. As observed previously for wild-type MTHFR at 25 °C (14), two phases could be detected in the Phe223Ala oxidative half-reaction. A fast phase, associated with ~84% of the total absorbance change, showed no clear dependence on the concentration of CH₂-H₄folate and yielded an observed rate

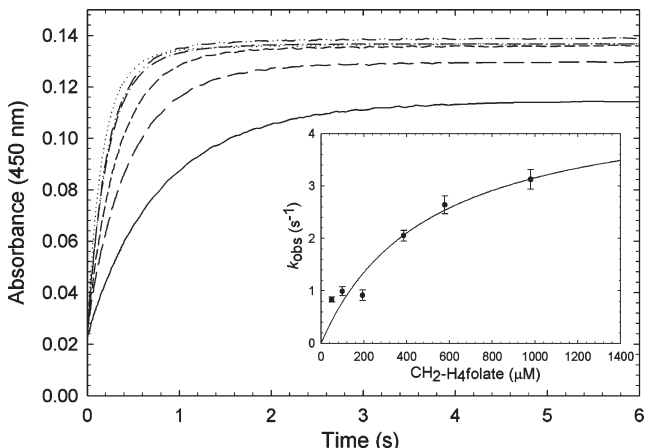


FIGURE 6: Reoxidation of the reduced Phe223Ala enzyme by CH₂-H₄folate. Photoreduced enzyme (10 μM) was mixed with solutions of 50 (—), 100 (---), 190 (--) 385 (-·-), 580 (-··-), and 980 μM (···) CH₂-H₄folate (concentrations after mixing). Stopped-flow reaction traces, monitored at 450 nm, were biphasic. The fast and slow phases accounted for 84 and 16%, respectively, of the total observed absorbance change. The inset shows the dependence of the slow phase on CH₂-H₄folate concentration. A hyperbolic fit of the data gave an apparent K_d of $500 \pm 230 \mu\text{M}$ for CH₂-H₄folate and a maximum rate constant of $4.5 \pm 1.1 \text{ s}^{-1}$. Reaction conditions were 50 mM potassium phosphate (pH 7.2) buffer containing 0.3 mM EDTA and 10% glycerol at 25 °C.

constant of 11 ± 2 s⁻¹ (data not shown). A slow phase, accounting for an ~16% increase in absorbance, was hyperbolically dependent on CH₂-H₄folate concentration, giving a maximal rate constant and an apparent K_d of 4.5 ± 1.1 s⁻¹ and 500 ± 230 μ M, respectively (inset of Figure 6 and Table 2). Thus, in comparison to the slow phase of oxidation for the wild-type enzyme (14), the Phe223Ala mutant has a 2-fold slower rate and a 45-fold decreased affinity for folate.

In the Physiological NADH-CH₂-H₄folate Oxidoreductase Reaction, the Phe223Leu and Phe223Ala Mutations Have Opposite Effects on Turnover. MTHFR oxidizes NADH to NAD⁺ and reduces CH₂-H₄folate to CH₃-H₄folate in the physiological NADH-CH₂-H₄folate oxidoreductase reaction, as shown in eq 1. To prevent oxidation of the CH₂-H₄folate substrate, the steady-state physiological assay is conducted under anaerobic conditions. Reactions with the Phe223Leu and Phe223Ala enzymes were performed at pH 7.2 and 25 °C. As indicated in Experimental Procedures, the data were fit either to eq 5, the Michaelis-Menten equation, or to eq 6 for single-substrate inhibition in a ping-pong bi-bi system (41). The kinetic parameters obtained for the two mutants are given in Table 3.

For the Phe223Leu variant, the maximum turnover number of $14 \pm 2 \text{ s}^{-1}$ (Table 3) is a slight increase over the value of $10.4 \pm 1.0 \text{ s}^{-1}$ determined for the wild-type enzyme (14). The observed k_{cat} for the mutant, 14 s^{-1} , is in reasonable agreement with the theoretical number of 17 s^{-1} that can be calculated from the maximal observed rate constants for the two half-reactions, reduction by NADH ($35 \pm 1 \text{ s}^{-1}$) and reoxidation by $\text{CH}_2\text{-H}_4\text{folate}$ ($34 \pm 1 \text{ s}^{-1}$) (Table 2), assuming a ping-pong bi-bi mechanism (49).

$$\frac{v}{[E_t]} = \frac{k_2' k_5'}{k_2' + k_5'} \text{ s}^{-1} = \frac{(35)(34)}{(35+34)} \text{ s}^{-1} = 17 \text{ s}^{-1} \quad (8)$$

Thus, the reductive and oxidative half-reactions are equally rate-determining in turnover for the Phe223Leu mutant enzyme.

These results stand in contrast to the physiological reaction catalyzed by the wild-type enzyme where the oxidative half-reaction involving CH₂-H₄folate is clearly rate-limiting (14).

For the Phe223Ala mutant, the k_{cat} of 2.9 s⁻¹ (Table 3) shows a 4-fold decrease compared to that of the wild-type enzyme. This observed turnover number is in reasonable agreement with the theoretical value of 4.0 s⁻¹, calculated from the maximal rate constants for the reductive half-reaction (40 ± 2 s⁻¹) and for the slow phase of the oxidative half-reaction (4.5 ± 1.1 s⁻¹) (Table 2).

$$\frac{v}{[E_t]} = \frac{k_2' k_{slow}}{k_2' + k_{slow}} \text{ s}^{-1} = \frac{(40)(4.5)}{(40 + 4.5)} \text{ s}^{-1} = 4.0 \text{ s}^{-1} \quad (9)$$

Thus, the reoxidation of the reduced enzyme by CH₂-H₄folate is rate-limiting in turnover for the Phe223Ala variant, as for wild-type MTHFR (14). Moreover, the slower of the two phases of reoxidation indeed limits the overall physiological reaction for the Phe223Ala mutant.

Structure of the Phe223Leu/Glu28Gln-CH₃-H₄folate Complex Provides Insight into the Contribution of Phe223 to Folate Binding. In previous work, we proposed that Glu28, located near N10 of the folate and in coordination with a water molecule (Figure 1), serves as the general acid catalyst in the oxidative half-reaction (32). Results with a Glu28Gln mutant supported this hypothesis. The mutation rendered the enzyme unable to catalyze the reduction of CH₂-H₄folate or the oxidation of CH₃-H₄folate in the reverse reaction. Evidence of CH₃-H₄folate binding was obtained by titration, however (32), and this property of the Glu28Gln variant was exploited in obtaining a structure of a folate-bound enzyme complex (23). To gain insight into the contribution of Phe223 to folate recognition in *E. coli* MTHFR, a double Phe223Leu/Glu28Gln mutant was produced, and a structure of the enzyme in complex with CH₃-H₄folate was determined (see the statistics in Table 1).

The 1.7 Å structure shows that the bound folate adopts an L-shaped conformation with its pterin ring parallel to the FAD isoalloxazine and perpendicular to the plane of the pABA group (Figure 7A). The distance of 3.6 Å between the N5-methyl of the folate and the N5 atom of the flavin suggests that the complex is competent for hydride transfer. Important polar residues interacting with the folate include Asp120, Gln183, Gln28, and Arg279 (Figure 7A). Asp120 and Gln183 participate in hydrogen bonding interactions with the pterin ring; Gln28, via a bridging water, hydrogen bonds to the N10 atom, and Arg279 interacts with the γ-carboxyl of the monoglutamate tail. The pABA ring sits in a hydrophobic box (the so-called “pABA pocket”) formed by Phe184, Leu212, Leu223, and Leu277 (Figure 7A).

The folate conformation and interactions with the protein are very similar to those observed in the structure of the Glu28Gln-CH₃-H₄folate complex (23). Figure 7B shows a superposition of the folate-bound Phe223Leu/Glu28Gln and Glu28Gln MTHFR structures. A notable difference between the two structures is that the folate rings interact less tightly with Leu223 than Phe223 (compare panels C and D of Figure 7). The contact surface area between the folate and Leu223 is only 44 Å², compared to 74 Å² for Phe223. Despite this difference, the overall protein-folate contact areas of the two complexes differ by less than 2% (556 Å² for Glu28Gln and 567 Å² for Phe223Leu/Glu28Gln) due to several small compensatory changes in protein-ligand surface area.

Folate binding is accompanied by conformational change in the protein. In Figure 8, the side chains of Gln219 and Leu223 from the ligand-free Phe223Leu and CH₃-H₄folate-bound

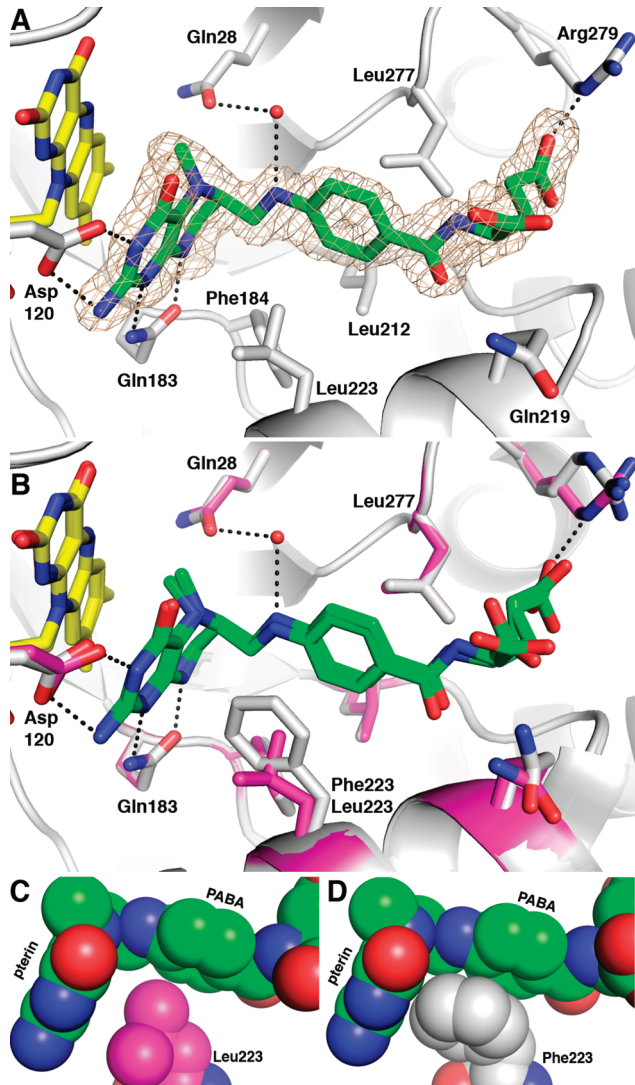


FIGURE 7: Active site of the Phe223Leu/Glu28Gln-CH₃-H₄folate complex. (A) Active site with electron density. The FAD and folate of the complex are colored yellow and green, respectively. Selected side chains are colored white. The map is a simulated annealing σ_A -weighted $F_o - F_c$ map contoured at 2σ. Prior to map calculation, the folate ligand was removed from the model and simulated annealing refinement was performed with PHENIX. (B) Superposition of the Phe223Leu/Glu28Gln-CH₃-H₄folate complex (magenta) and the Glu28Gln-CH₃-H₄folate complex (white, PDB entry 1zp4). (C) Close-up view of the interactions between Leu223 and the folate in the Phe223Leu/Glu28Gln-CH₃-H₄folate complex. (D) Close-up view of the interactions between Phe223 and the folate in the Glu28Gln-CH₃-H₄folate complex (PDB entry 1zp4).

Phe223Leu/Glu28Gln structures are superimposed. In the absence of ligand, Leu223 occludes the binding pocket for the pABA ring while Gln219 blocks the site to be occupied by the α-carboxylate. Upon binding, Leu223 and Gln219 apparently rotate around their respective C_α-C_β bond vectors to allow the folate to enter. Analogous movements of Phe223 and Gln219 occur for the Glu28Gln mutant enzyme (23). Thus, the substitution of Leu for Phe at position 223 has not impaired the conformational changes needed for folate binding.

DISCUSSION

Phe223 Has a Major Role in NADH Binding. Compared to the multiple interactions commonly observed for protein-

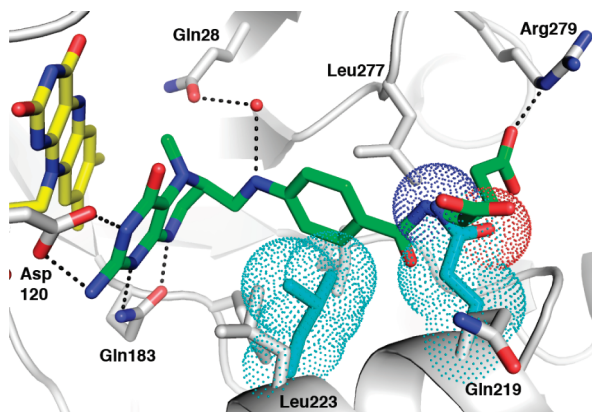


FIGURE 8: Conformational changes induced by the binding of $\text{CH}_3\text{-H}_4\text{folate}$. The structure of the Phe223Leu/Glu28Gln- $\text{CH}_3\text{-H}_4\text{folate}$ complex is colored white with yellow FAD and green folate. The side chains of Gln219 and Leu223 of the ligand-free Phe223Leu structure are colored cyan with accompanying van der Waals dot surfaces. Note that these surfaces overlap with the $\text{CH}_3\text{-H}_4\text{folate}$.

NAD(P)H complexes, NADH bound to *E. coli* MTHFR makes few contacts with the protein (23). Only three amino acids, Gln183, Thr59, and Glu28, participate in hydrogen bonding to the substrate. The most significant contributions to NADH binding are, therefore, stacking and hydrophobic interactions. We have proposed that Phe223 serves an important function in supporting the stacked conformation of the NADH (Figure 1) and, thus, would likely play a key role in the reductive half-reaction of the enzyme. To investigate the function of this amino acid, we have characterized mutants Phe223Leu and Phe223Ala, which differ in aromaticity and hydrophobicity from Phe223.

Although the Phe223Leu and Phe223Ala enzymes catalyze the reductive half-reaction at rates similar to that of the wild-type enzyme (Table 2), the variants bind the NADH substrate considerably less tightly than does wild-type MTHFR. Replacement of Phe223 with Ala increased the K_d for NADH by 40-fold, whereas replacement with Leu increased the K_d by 14-fold (Table 2). For the Phe223Ala mutant, a change in standard free binding energy of 2.2 kcal/mol is calculated from the observed 40-fold increase in K_d for NADH (at 298 K). Since the mean volumes of Phe (193.5 \AA^3) and Ala (90.1 \AA^3) (28) differ significantly, this change may be attributed to lost hydrophobic interactions between the Phe223Ala enzyme and the NADH substrate. Entropic effects may also be involved, however. From partitioning experiments, the substitution of an Ala for a Phe decreases the hydrophobicity by 2 kcal/mol (50), which suggests that the loss of hydrophobic interactions may, indeed, account for the lost binding energy of 2.2 kcal/mol observed in the Phe223Ala mutant. A similar analysis applied to Phe223Leu MTHFR reveals a change in the binding energy of 1.6 kcal/mol (at 298 K) corresponding to the 14-fold increase in K_d . The difference in hydrophobicity between Phe and Leu is only 0.7 kcal/mol from partitioning experiments (50). Thus, for the Phe223Leu mutant, we estimate that the remaining 0.9 kcal/mol of the observed binding energy change may be attributed to lost $\pi-\pi$ aromatic stacking between the Phe side chain and the adenine of NADH. Consistent with this view, a mean potential energy of 1.3 kcal/mol has been reported for an aromatic–aromatic pair interaction within a set of 34 proteins (51). Taken together, our results with the Phe223Ala and Phe223Leu mutants suggest that both hydrophobicity and aromaticity make major

contributions to the binding of stacked NADH in bacterial MTHFR.

At least five examples of folded pyridine nucleotides in flavoproteins other than *E. coli* MTHFR have been reported (52–56). Like MTHFR, two of the structures, PheA2, the flavin reductase component of a two-protein-requiring phenol hydroxylase system from *Bacillus thermoglucosidasius* A7 (54), and HpaC, the flavin reductase of a two-component 4-hydroxyphenylacetate 3-monoxygenase from *Thermus thermophilus* (56), reveal a folded NAD stacked upon the isoalloxazine of FAD, in an orientation competent for hydride transfer. In neither enzyme is there a parallel stacking between the adenine of the bound NAD and a Phe amino acid, as observed in MTHFR. The affinity for NADH does not appear to be significantly different than in MTHFR, however. While no K_d values are available, a K_m for NADH of $8.8 \mu\text{M}$ at 53°C for PheA2 (57) and a K_m of $36.8 \mu\text{M}$ at 30°C for HpaC from *T. thermophilus* (56) have been reported, in comparison with a K_d for NADH of $32 \mu\text{M}$ and a K_m of $20 \mu\text{M}$ in the physiological reaction at 25°C for MTHFR (14). Thus, precedence exists for a stacked NADH conformation without a parallel Phe or another aromatic amino acid in the outer layer of the sandwich.

The data presented in this paper are consistent with a role for Phe223 in supporting the stacked conformation of the NADH in *E. coli* MTHFR. Considering our results, however, it is interesting that Phe223 is not completely conserved within MTHFRs. We produced the Phe223Leu mutant of *E. coli* MTHFR to emulate the human enzyme, yet the mutation significantly lowers the apparent affinity for NADH (Table 2). Moreover, the Phe223Leu enzyme has no ability to bind NADPH (data not shown), the preferred substrate for human/pig MTHFR. Three-dimensional structures of mammalian MTHFR and Phe223Leu *E. coli* MTHFR in complex with NADH have not been determined to help explain our results. An alignment of the bacterial and human MTHFR sequences shows no striking differences in any of the amino acids lining the pyridine nucleotide-binding site. Thus, further biochemical and structural studies on both the human and bacterial enzymes are needed to elucidate their differences in pyridine nucleotide binding.

Phe223 Participates in Folate Binding. Phe223 stacks tightly against the adenine ring of the pyridine nucleotide in the NADH complex, but it swings out to lie over the pABA ring in the folate complex (Figure 1) (23). This active movement of the Phe aromatic side chain toward the pABA moiety to participate in $\pi-\pi$ stacking suggests a functional role for Phe223 in folate binding. To test our hypothesis, we have examined the affinity of mutants Phe223Leu and Phe223Ala for $\text{CH}_2\text{-H}_4\text{folate}$ during the oxidative half-reaction at 25°C . Our results show that substitution of Phe223 with Leu does not change the apparent K_d for $\text{CH}_2\text{-H}_4\text{folate}$ (Figure 5 and Table 2). By contrast, the Phe223Ala mutation reduces the affinity for $\text{CH}_2\text{-H}_4\text{folate}$ by 45-fold (Figure 6 and Table 2). This decrease corresponds to an observed change in standard free binding energy of 2.3 kcal/mol, a value comparable to the reported 2 kcal/mol difference in hydrophobicity effected by a Phe to Ala substitution (50). Although there may be other contributions, such as entropic differences, to the observed loss in binding energy, our data suggest that the decrease in the level of folate binding by the Phe223Ala enzyme may be largely attributed to lost hydrophobic interactions between the Ala amino acid and the substrate $\text{CH}_2\text{-H}_4\text{folate}$.

Relevant to this work on MTHFR, $\pi-\pi$ stacking interactions between an aromatic residue and the *p*ABA ring of folate have also been observed in the folate-dependent enzyme, human methylenetetrahydrofolate dehydrogenase/cyclohydrolase (58). Mammals have a cytosolic trifunctional enzyme containing three activities: (1) methylenetetrahydrofolate dehydrogenase, (2) methenyltetrahydrofolate cyclohydrolase, and (3) 10-formyltetrahydrofolate synthetase. The structure of the bifunctional dehydrogenase/cyclohydrolase domain of the human trifunctional enzyme, in complex with folate inhibitor Ly345899, revealed a conserved tyrosine residue (Tyr52) that stacks against the *p*ABA ring of the folate (58), in a manner similar to the stacking of Phe223 in the CH₃-H₄folate structure of MTHFR. Tyr52Ala and Tyr52Phe variants of the bifunctional enzyme have been prepared and the K_m values for CH₂-H₄folate measured in the dehydrogenase assay. Binding information, however, is likely not reflected in the K_m values, as the K_m was unchanged for the Tyr52Ala variant but increased 10-fold for the Tyr52Phe enzyme (58).

As revealed in the Glu28Gln-CH₃-H₄folate structure (23), the *p*ABA ring of folate is actually surrounded by three hydrophobic residues, Phe184, Leu212, and Leu277, in addition to Phe223. In our Phe223Leu/Glu28Gln-CH₃-H₄folate complex, Leu takes the place of Phe223 as one wall of this “*p*ABA pocket” (Figure 7A). Notably, hydrophobic *p*ABA pockets have been observed in two other folate-dependent enzymes: (1) thymidylate synthase (59–61) and (2) dihydrofolate reductase (DHFR) (62, 63), which catalyzes the NADPH-linked reduction of H₂folate to H₄folate. However, none of the residues lining the *p*ABA pocket in these enzymes stacks directly parallel onto the aromatic ring as Phe223 does in bacterial MTHFR. Mutational studies have been performed on two invariant residues in the *p*ABA pocket of *E. coli*/human dihydrofolate reductase: Phe31/Phe34 and Leu54/Leu67. Compared to the Phe223Ala and Phe223Leu variants of *E. coli* MTHFR, larger effects on folate affinity were observed. The apparent K_d for H₂folate was increased 125-fold in a Phe31Ala human DHFR mutant (64) and 25-fold in a Phe31Val mutant of the *E. coli* enzyme (65). Leu54Gly and Leu54Ile *E. coli* DHFRs demonstrated 1700- and 10-fold decreases in H₂folate affinity, respectively (66). In each of these mutants, the higher K_d values were predominantly the result of faster off rates of H₂folate.

The Phe223Leu Mutation Improves Folate Catalysis in MTHFR. Our studies of the oxidative half-reaction show that while the Phe223Ala mutation slowed folate catalysis by 2-fold (Figure 6 and Table 2), the Phe223Leu mutation actually increased the rate of CH₂-H₄folate-dependent flavin oxidation by 3-fold (Figure 6 and Table 2). Overall, these changes are small, probably because Phe223 is more than 11 Å from the site of hydride transfer in MTHFR. An interesting result obtained with the Phe223Leu mutant is that the enzyme catalyzes flavin oxidation in one phase (Figure 5), in contrast to the two phases observed for the wild-type enzyme (14, 33) and for the Phe223Ala variant (Figure 6). We have previously proposed two possible mechanisms to explain the two phases of oxidation (33). However, until we understand the origin of the biphasic oxidation by wild-type MTHFR, we will not be able to interpret the factors leading to the observed differences between the Phe223Leu and wild-type enzymes.

Our examination of Phe223Ala MTHFR in folate catalysis can be compared to a mutational study on Tyr52, which participates in $\pi-\pi$ stacking with the *p*ABA ring in the bifunctional methylenetetrahydrofolate dehydrogenase/cyclohydrolase.

The 2-fold effect observed for the Phe223Ala mutation in MTHFR wanes in comparison to a 100-fold decrease in specific activity observed for the Tyr52Ala substitution in the dehydrogenase/cyclohydrolase (58). However, to understand the large catalytic discrepancy between these mutant enzymes, more comprehensive kinetic studies need to be performed on the bifunctional enzyme. The rates of hydride transfer have been measured in mutational studies of the residues lining the DHFR *p*ABA pocket, and these can be more directly compared to the k_5' values of Phe223Ala and Phe223Leu MTHFRs (Table 2). Again, larger effects were observed in DHFR than in MTHFR. Mutants Leu54Ile and Leu54Gly of *E. coli* DHFR exhibited 30-fold decreases in the level of hydride transfer (66), and mutants Phe31Val and Phe31Ala of the human enzyme showed decreases of 25- and 200-fold, respectively (64).

Since the Phe223Leu mutant of *E. coli* MTHFR was constructed, in part, to mimic the mammalian enzyme, it is useful to compare the oxidative half-reaction catalyzed by the mutant to that of pig liver MTHFR (13). Under the same conditions, 25 °C and pH 7.2, the porcine enzyme binds CH₂-H₄folate with 8-fold less affinity and catalyzes the folate half-reaction at a slightly faster rate than the Phe223Leu *E. coli* mutant. Thus, factors in addition to the amino acid at the 223 position are influencing folate binding and catalysis. Although no three-dimensional structures of a mammalian MTHFR are available, a comparison of the bacterial and human MTHFR sequences shows only conservative changes in the amino acids of the folate-binding site. For example, *p*ABA pocket residues Leu212 and Phe184 of *E. coli* MTHFR are replaced with a Phe and a Leu, respectively, in the human enzyme. Other substitutions include three amino acids that form a hydrogen bond to Phe223 in the bacterial enzyme. Such modest changes are difficult to reconcile with the observed differences between mammalian and bacterial MTHFRs.

In summary, our results suggest significant roles for Phe223 in NADH and folate binding. Moreover, our data demonstrate that the Phe223Leu mutant binds folate and catalyzes the oxidative half-reaction similar to the wild-type *E. coli* enzyme, suggesting a possible rationale for the occurrence of Leu at this position in some MTHFRs.

ACKNOWLEDGMENT

We dedicate this paper to the late Dr. Martha L. Ludwig. We acknowledge Merck Eprova AG for the gifts of folate compounds. We thank Dr. Jay Nix of Advanced Light Source beamline 4.2.2 for help with data collection. The Advanced Light Source is supported by the Director, Office of Science, Office of Basic Energy Sciences, of the U.S. Department of Energy under Contract DE-AC02-05CH11231. We acknowledge Robert Pejchal, Bruce Palfey, Vahe Bandarian, and Rowena Matthews for helpful discussions.

SUPPORTING INFORMATION AVAILABLE

Methods describing the simulations of the Phe223Leu oxidative half-reaction and a plot of the simulated traces. This material is available free of charge via the Internet at <http://pubs.acs.org>.

REFERENCES

- Jacques, P. F., Bostom, A. G., Williams, R. R., Ellison, R. C., Eckfeldt, J. H., Rosenberg, I. H., Selhub, J., and Rozen, R. (1996) Relation between folate status, a common mutation in methylenetetrahydrofolate dehydrogenase/cyclohydrolase

- reductase, and plasma homocysteine concentrations. *Circulation* 93, 7–9.
2. Chen, Z., Karaplis, A. C., Ackerman, S. L., Pogribny, I. P., Melnyk, S., Lussier-Cacan, S., Chen, M. F., Pai, A., John, S. W. M., Smith, R. S., Bottiglieri, T., Bagley, P., Selhub, J., Rudnicki, M. A., James, S. J., and Rozen, R. (2001) Mice deficient in methylenetetrahydrofolate reductase exhibit hyperhomocysteinemia and decreased methylation capacity, with neuropathology and aortic lipid deposition. *Hum. Mol. Genet.* 10, 433–443.
 3. Refsum, H., Ueland, P. M., Nygard, O., and Vollset, S. E. (1998) Homocysteine and Cardiovascular Disease. *Annu. Rev. Med.* 49, 31–62.
 4. McCaddon, A., Davies, G., Hudson, P., Tandy, S., and Cattell, H. (1998) Total serum homocysteine in senile dementia of Alzheimer type. *Int. J. Geriatr. Psychiatry* 13, 235–239.
 5. Clarke, R., Smith, A. D., Jobst, K. A., Refsum, H., Sutton, L., and Ueland, P. M. (1998) Folate, vitamin B₁₂, and serum total homocysteine levels in confirmed Alzheimer disease. *Arch. Neurol.* 55, 1449–1455.
 6. Seshadri, S., Beiser, A., Selhub, J., Jacques, P. F., Rosenberg, I. H., D'Agostino, R. B., Wilson, P. W., and Wolf, P. A. (2002) Plasma homocysteine as a risk factor for dementia and Alzheimer's disease. *N. Engl. J. Med.* 346, 476–483.
 7. van der Put, N. M. J., van Straaten, H. W. M., Trijbels, F. J. M., and Blom, H. J. (2001) Folate, Homocysteine and Neural Tube Defects: An Overview. *Exp. Biol. Med.* 226, 243–270.
 8. Matthews, R. G. (2002) Methylenetetrahydrofolate reductase: A common human polymorphism and its biochemical implications. *Chem. Rec.* 2, 4–12.
 9. Raymond, R. K., Kastanos, E. K., and Appling, D. R. (1999) *Saccharomyces cerevisiae* expresses two genes encoding isozymes of methylenetetrahydrofolate reductase. *Arch. Biochem. Biophys.* 372, 300–308.
 10. Roje, S., Wang, H., McNeil, S. D., Raymond, R. K., Appling, D. R., Schachar-Hill, Y., Bohnert, H. J., and Hanson, A. D. (1999) Isolation, characterization, and functional expression of cDNAs encoding NADH-dependent methylenetetrahydrofolate reductase from higher plants. *J. Biol. Chem.* 274, 36089–36096.
 11. Roje, S., Chan, S. Y., Kaplan, F., Raymond, R. K., Horne, D. W., Appling, D. R., and Hanson, A. D. (2002) Metabolic engineering in yeast demonstrates that S-adenosylmethionine controls flux through the methylenetetrahydrofolate reductase reaction *in vivo*. *J. Biol. Chem.* 277, 4056–4061.
 12. Vickers, T. J., Orsomando, G., de la Garza, R. D., Scott, D. A., Kang, S. O., Hanson, A. D., and Beverley, S. M. (2006) Biochemical and genetic analysis of methylenetetrahydrofolate reductase in *Leishmania* metabolism and virulence. *J. Biol. Chem.* 281, 38150–38158.
 13. Vanoni, M. A., Ballou, D. P., and Matthews, R. G. (1983) Methylenetetrahydrofolate reductase: Steady state and rapid reaction studies on the NADPH-methylenetetrahydrofolate, NADPH-menadione, and methyltetrahydrofolate-menadione oxidoreductase activities of the enzyme. *J. Biol. Chem.* 258, 11510–11514.
 14. Trimmer, E. E., Ballou, D. P., and Matthews, R. G. (2001) Methylenetetrahydrofolate reductase from *Escherichia coli*: Elucidation of the kinetic mechanism by steady-state and rapid-reaction studies. *Biochemistry* 40, 6205–6215.
 15. Matthews, R. G., and Haywood, B. J. (1979) Inhibition of pig liver methylenetetrahydrofolate reductase by dihydrofolate: Some mechanistic and regulatory implications. *Biochemistry* 18, 4845–4851.
 16. Sumner, J. S., and Matthews, R. G. (1992) Stereochemistry and mechanism of hydrogen transfer between NADPH and methylenetetrahydrofolate in the reaction catalyzed by methylenetetrahydrofolate reductase from pig liver. *J. Am. Chem. Soc.* 114, 6949–6956.
 17. Vanoni, M. A., and Matthews, R. G. (1984) Kinetic isotope effects on the oxidation of reduced nicotinamide adenine dinucleotide phosphate by the flavoprotein methylenetetrahydrofolate reductase. *Biochemistry* 23, 5272–5279.
 18. Vanoni, M. A., Lee, S., Floss, H. G., and Matthews, R. G. (1990) Stereochemistry of reduction of methylenetetrahydrofolate to methyltetrahydrofolate catalyzed by pig liver methylenetetrahydrofolate reductase. *J. Am. Chem. Soc.* 112, 3987–3992.
 19. Kallen, R. G., and Jencks, W. P. (1966) The mechanism of the condensation of formaldehyde with tetrahydrofolic acid. *J. Biol. Chem.* 241, 5845–5850.
 20. Perry, K. M., Carreras, C. W., Chang, L. C., Santi, D. V., and Stroud, R. M. (1993) Structures of thymidylate synthase with a C-terminal deletion: Role of the C-terminus in alignment of 2'-deoxyuridine 5'-monophosphate and 5,10-methylenetetrahydrofolate. *Biochemistry* 32, 7116–7125.
 21. Sheppard, C. A., Trimmer, E. E., and Matthews, R. G. (1999) Purification and properties of NADH-dependent 5,10-methylenetetrahydrofolate reductase (MetF) from *Escherichia coli*. *J. Bacteriol.* 181, 718–725.
 22. Guenther, B. D., Sheppard, C. A., Tran, P., Rozen, R., Matthews, R. G., and Ludwig, M. L. (1999) The structure and properties of methylenetetrahydrofolate reductase from *Escherichia coli* suggest how folate ameliorates human hyperhomocysteinemia. *Nat. Struct. Biol.* 6, 359–365.
 23. Pejchal, R., Sargeant, R., and Ludwig, M. L. (2005) Structures of NADH and CH₃-H₄folate Complexes of *Escherichia coli* Methylenetetrahydrofolate Reductase Reveal a Spartan Strategy for a Ping-Pong Reaction. *Biochemistry* 44, 11447–11457.
 24. Pejchal, R., Campbell, E., Guenther, B. D., Lennon, B. W., Matthews, R. G., and Ludwig, M. L. (2006) Structural perturbations in the Ala → Val polymorphism of methylenetetrahydrofolate reductase: How binding of folates may protect against inactivation. *Biochemistry* 45, 4808–4818.
 25. Altschul, S. F., Madden, T. L., Schaffer, A. A., Zhang, J., Zhang, Z., Miller, W., and Lipman, D. J. (1997) Gapped BLAST and PSI-BLAST: A new generation of protein database search programs. *Nucleic Acids Res.* 25, 3389–3402.
 26. Thompson, J. D., Higgins, D. G., and Gibson, T. J. (1994) CLUSTAL W: Improving the sensitivity of progressive multiple sequence alignment through sequence weighting, position-specific gap penalties and weight matrix choice. *Nucleic Acids Res.* 22, 4673–4680.
 27. Larkin, M. A., Blackshields, G., Brown, N. P., Chenna, R., McGgettigan, P. A., McWilliam, H., Valentin, F., Wallace, I. M., Wilm, A., Lopez, R., Thompson, J. D., Gibson, T. J., and Higgins, D. G. (2007) Clustal W and clustal X version 2.0. *Bioinformatics* 23, 2947–2948.
 28. Harpaz, Y., Gerstein, M., and Chothia, C. (1994) Volume changes on protein folding. *Structure* 2, 641–649.
 29. Bull, C., and Ballou, D. P. (1981) Purification and properties of protocatechuic 3,4-dioxygenase from *Pseudomonas putida*. A new iron to subunit stoichiometry. *J. Biol. Chem.* 256, 12673–12680.
 30. Fasman, G. D. (1976) *Handbook of Biochemistry and Molecular Biology*, 3rd ed., Vol. I, CRC Press, Inc., Cleveland, OH.
 31. Blakley, R. L. (1969) *The Biochemistry of Folic Acid and Related Pteridines*, North-Holland, Amsterdam.
 32. Trimmer, E. E., Ballou, D. P., Ludwig, M. L., and Matthews, R. G. (2001) Folate activation and catalysis in methylenetetrahydrofolate reductase from *Escherichia coli*: Roles for aspartate 120 and glutamate 28. *Biochemistry* 40, 6216–6226.
 33. Trimmer, E. E., Ballou, D. P., Galloway, L. J., Scannell, S. A., Brinker, D. R., and Casas, K. R. (2005) Aspartate 120 of *Escherichia coli* methylenetetrahydrofolate reductase: Evidence for major roles in folate binding and catalysis and a minor role in flavin reactivity. *Biochemistry* 44, 6809–6822.
 34. Massey, V. (1991) A simple method for the determination of redox potentials. In *Flavins and Flavoproteins 1990* (Curti, B., Ronchi, S., and Zanetti, G., Eds.) pp 59–66, Walter de Gruyter & Co., Berlin.
 35. Clark, W. M. (1960) *Oxidation-Reduction Potentials of Organic Systems*, Williams & Wilkins Co., Baltimore.
 36. Patil, P. V., and Ballou, D. P. (2000) The use of protocatechuic dioxygenase for maintaining anaerobic conditions in biochemical experiments. *Anal. Biochem.* 286, 187–192.
 37. Press, W. H., Teulosky, S. A., Vetterling, W. T., and Flannery, B. P. (1992) *Numerical methods in C*, 2nd ed., Cambridge University Press, Cambridge, U.K.
 38. Donaldson, K. O., and Keresztesy, J. C. (1962) Naturally occurring forms of folic acid. II. Enzymatic conversion of methylenetetrahydrofolic acid to prefolic A-methyltetrahydrofolate. *J. Biol. Chem.* 237, 1298–1304.
 39. Matthews, R. G. (1986) Methylenetetrahydrofolate reductase from pig liver. *Methods Enzymol.* 122, 372–381.
 40. Kutzbach, C., and Stokstad, E. L. R. (1971) Mammalian methylenetetrahydrofolate reductase: Partial purification, properties, and inhibition by S-adenosylmethionine. *Biochim. Biophys. Acta* 250, 459–477.
 41. Cleland, W. W. (1979) Substrate Inhibition. *Methods Enzymol.* 63, 500–513.
 42. Pflugrath, J. W. (1999) The finer things in X-ray diffraction data collection. *Acta Crystallogr. D55*, 1718–1725.
 43. Engh, R. A., and Huber, R. (1991) Accurate bond and angle parameters for X-ray protein structure refinement. *Acta Crystallogr. A47*, 392–400.
 44. Lovell, S. C., Davis, I. W., Arendall, W. B. III, de Bakker, P. I., Word, J. M., Prisant, M. G., Richardson, J. S., and Richardson, D. C. (2003) Structure validation by Cα geometry: φ, ψ, and Cβ deviation. *Proteins* 50, 437–450.
 45. Adams, P. D., Grosse-Kunstleve, R. W., Hung, L. W., Ioerger, T. R., McCoy, A. J., Moriarty, N. W., Read, R. J., Sacchettini, J. C., Sauter, N. K., and Terwilliger, T. C. (2002) PHENIX: Building new software

- for automated crystallographic structure determination. *Acta Crystallogr. D* 58, 1948–1954.
46. Zwart, P. H., Afonine, P. V., Grosse-Kunstleve, R. W., Hung, L. W., Ioerger, T. R., McCoy, A. J., McKee, E., Moriarty, N. W., Read, R. J., Saccoccini, J. C., Sauter, N. K., Storoni, L. C., Terwilliger, T. C., and Adams, P. D. (2008) Automated structure solution with the PHENIX suite. *Methods Mol. Biol.* 426, 419–435.
 47. Emsley, P., and Cowtan, K. (2004) Coot: Model-building tools for molecular graphics. *Acta Crystallogr. D* 60, 2126–2132.
 48. Cleland, W. W. (1975) Partition analysis and the concept of net rate constants as tools in enzyme kinetics. *Biochemistry* 14, 3220–3224.
 49. Massey, V., Gibson, Q. H., and Veeger, C. (1960) Intermediates in the catalytic action of lipoyl dehydrogenase (diaphorase). *Biochem. J.* 77, 341–351.
 50. Nozaki, Y., and Tanford, C. (1971) The solubility of amino acids and two glycine peptides in aqueous ethanol and dioxane solutions: Establishment of a hydrophobicity scale. *J. Biol. Chem.* 246, 2211–2217.
 51. Burley, S. K., and Petsko, G. A. (1985) Aromatic-aromatic interaction: A mechanism of protein structure stabilization. *Science* 229, 23–28.
 52. Tanner, J. J., Tu, S.-C., Barbour, L. J., Barnes, C. L., and Krause, K. L. (1999) Unusual folded conformation of nicotinamide adenine dinucleotide bound to flavin reductase P. *Protein Sci.* 8, 1725–1732.
 53. Singh, S. K., Kurnasov, O. V., Chen, B., Robinson, H., Grishin, N. V., Osterman, A. L., and Zhang, H. (2002) Crystal structure of *Haemophilus influenzae* NadR protein: A bifunctional enzyme endowed with NMN adenyllyltransferase and ribosylnicotinamide kinase activities. *J. Biol. Chem.* 277, 33291–33299.
 54. van den Heuvel, R. H. H., Westphal, A. H., Heck, A. J. R., Walsh, M. A., Rovida, S., van Berkel, W. J. H., and Mattevi, A. (2004) Structural studies of flavin reductase PheA2 reveal binding of NAD in an unusual folded conformation and support novel mechanism of action. *J. Biol. Chem.* 279, 12860–12867.
 55. Okai, M., Kudo, N., Lee, W. C., Kamo, M., Nagata, K., and Tanokura, M. (2006) Crystal structures of the short-chain flavin reductase HpaC from *Sulfolobus tokodaii* strain 7 in its three states: NAD(P)⁺-free, NAD⁺-bound, and NADP⁺-bound. *Biochemistry* 45, 5103–5110.
 56. Kim, S. H., Hisano, T., Iwasaki, W., Ebihara, A., and Miki, K. (2007) Crystal structure of the flavin reductase component (HpaC) of 4-hydroxyphenylacetate 3-monooxygenase from *Thermus thermophilus* HB8: Structural basis for the flavin affinity. *Proteins* 70, 718–730.
 57. Kirchner, U., Westphal, A. H., Muller, R., and van Berkel, W. J. H. (2003) Phenol hydroxylase from *Bacillus thermoglucosidasius* A7, a two-protein component monooxygenase with a dual role for FAD. *J. Biol. Chem.* 278, 47545–47553.
 58. Schmidt, A., Wu, H., MacKenzie, R. E., Chen, V. J., Bewly, J. R., Ray, J. E., Toth, J. E., and Cygler, M. (2000) Structures of three inhibitor complexes provide insight into the reaction mechanism of the human methylenetetrahydrofolate dehydrogenase/cyclohydro-lase. *Biochemistry* 39, 6325–6335.
 59. Matthews, D. A., Appelt, K., Oatley, S. J., and Xuong, N. H. (1990) Crystal structure of *Escherichia coli* thymidylate synthase containing bound 5-fluoro-2'-deoxyuridylate and 10-propargyl-5,8-dideazafo-late. *J. Mol. Biol.* 214, 923–936.
 60. Montfort, W. R., Perry, K. M., Fauman, E. B., Finer-Moore, J. S., Maley, G. F., Hardy, L., Maley, F., and Stroud, R. M. (1990) Structure, multiple site binding, and sequential accommodation in thymidylate synthase on binding dUMP and anti-folate. *Biochemistry* 29, 6964–6977.
 61. Sayre, P. H., Finer-Moore, J. S., Fritz, T. A., Biermann, D., Gates, S. B., MacKellar, W. C., Patel, V. F., and Stroud, R. M. (2001) Multi-targeted antifolates aimed at avoiding drug resistance form covalent closed inhibitory complexes with human and *Escherichia coli* thymidylate synthases. *J. Mol. Biol.* 313, 813–829.
 62. Bolin, J. T., Filman, D. J., Matthews, D. A., Hamlin, R. C., and Kraut, J. (1982) Crystal structures of *Escherichia coli* and *Lactobacillus casei* dihydrofolate reductase refined at 1.7 Å resolution. *J. Biol. Chem.* 257, 13650–13662.
 63. Oefner, C., D'Arcy, A., and Winkler, F. K. (1988) Crystal structure of human dihydrofolate reductase complexed with folate. *Eur. J. Biochem.* 174, 377–385.
 64. Nakano, T., Spencer, H. T., Appleman, J. R., and Blakley, R. L. (1994) Critical role of phenylalanine 34 of human dihydrofolate reductase in substrate and inhibitor binding and in catalysis. *Biochemistry* 33, 9945–9952.
 65. Chen, J.-T., Taira, K., Tu, C.-P. D., and Benkovic, S. J. (1987) Probing the functional role of phenylalanine-31 of *Escherichia coli* dihydrofolate reductase by site-directed mutagenesis. *Biochemistry* 26, 4093–4100.
 66. Murphy, D. J., and Benkovic, S. J. (1989) Hydrophobic interactions via mutants of *Escherichia coli* dihydrofolate reductase: Separation of binding and catalysis. *Biochemistry* 28, 3025–3031.